

Study of the magnetic penetration depth in RbOs_2O_6

R. Khasanov,^{1,2,3} D.G. Eshchenko,^{3,4} D. Di Castro,^{3,5} A. Shengelaya,³ F. La Mattina,³
A. Maisuradze,³ C. Baines,⁴ H. Luetkens,⁴ J. Karpinski,⁶ S.M. Kazakov,⁶ and H. Keller³

¹ *Laboratory for Neutron Scattering, ETH Zürich and Paul Scherrer Institut, CH-5232 Villigen PSI, Switzerland*

² *DPMC, Université de Genève, 24 Quai Ernest-Ansermet, 1211 Genève 4, Switzerland*

³ *Physik-Institut der Universität Zürich, Winterthurerstrasse 190, CH-8057, Zürich, Switzerland*

⁴ *Laboratory for Muon Spin Spectroscopy, PSI, CH-5232 Villigen PSI, Switzerland*

⁵ *Coherencia-INFM and Department of Physics, University of Rome "La Sapienza"*

⁶ *Solid State Physics Laboratory, ETH 8093 Zürich, Switzerland*

Measurements of the magnetic field penetration depth λ in the pyrochlore superconductor RbOs_2O_6 ($T_c \simeq 6.3$ K) were carried out by means of the muon-spin-rotation (μSR) technique. At low temperatures $\lambda^{-2}(T)$ saturates and becomes constant below $T \simeq 0.2T_c$, in agreement with what is expected for weak-coupled s-wave BCS superconductors. The value of λ at $T = 0$ was found to be in the range of 250 nm to 300 nm. μSR and equilibrium magnetization measurements both reveal that at low temperatures λ is almost (at the level of 10%) independent of the applied magnetic field. This result suggests that the superconducting energy gap in RbOs_2O_6 is isotropic.

PACS numbers: 74.70.Dd, 74.25.Op, 74.25.Ha, 76.75.+i, 83.80.Fg

I. INTRODUCTION

The discovery of superconductivity in pyrochlore related oxides has attracted considerable interest in the study of these materials.^{1,2,3,4,5,6,7,8} However, till now there is no agreement about the nature of superconducting pairing mechanism in these compounds. From the one hand, based on the results of the specific heat,⁹ nuclear quadrupole resonance (NQR)¹⁰ and muon-spin rotation (μSR)^{11,12} experiments, $\text{Cd}_2\text{Re}_2\text{O}_7$ is suggested to be a weak-coupled isotropic BCS superconductor. Specific heat,⁵ pressure effect on the magnetic field penetration depth¹³ and nuclear magnetic resonance (NMR)¹⁴ measurements of RbOs_2O_6 and the band structure calculations of KOs_2O_6 ¹⁵ also point to the conventional type of superconductivity. From the other hand, second critical field H_{c2} ,⁴ μSR ,^{11,16} and specific heat⁴ measurements suggest an unconventional type of pairing in KOs_2O_6 and RbOs_2O_6 .

The magnetic field penetration depth λ is one of the fundamental lengths of a superconductor. The temperature dependence $\lambda(T)$ reflects the quasiparticle density of states available for thermal excitations and therefore probes the superconducting gap structure. The shape of $\lambda(T)$ and the zero-temperature value $\lambda(0)$ provide information about the superconducting mechanism and set a length scale for the screening of an external magnetic field. In addition, the field dependence of λ at low temperatures may reflect the anisotropy of the superconducting energy gap.^{11,17} In this paper, we report on magnetic field penetration depth measurements down to 30 mK in RbOs_2O_6 by means of the transverse-field muon-spin rotation (TF- μSR) technique (see e.g. [18]). The temperature dependence of λ^{-2} saturates at low temperatures and becomes constant below $T \simeq 0.2T_c$. This behavior agrees with what is expected for weak-coupled s-wave

BCS superconductors. Measurements of the magnetic field dependence of λ by means of TF- μSR and magnetization reveal that at low temperatures λ is almost field independent. This result suggests that the superconducting energy gap in RbOs_2O_6 is isotropic. The ratio $2\Delta_0/k_B T_c$ was found to be in the range of 3.09–3.98, which is close to the weak-coupling BCS value 3.52.

The paper is organized as follows: In Sec. II we describe the sample preparation procedure and the TF- μSR technique as a tool to measure the magnetic field penetration depth λ . Sec. III A comprises studies of the temperature dependence of λ . In Secs. III B and III C we discuss the calculation of the absolute value of λ and its magnetic field dependence. In Sec. III D results on the dependence of the zero-temperature superconducting gap Δ_0 on the superconducting critical temperature and the magnetic field are reported. The conclusions follow in Sec. IV.

II. SAMPLE PREPARATION AND EXPERIMENTAL TECHNIQUES

A. Sample preparation

Polycrystalline samples of RbOs_2O_6 were synthesized by a procedure similar to that described in Refs. [3,5,6]. A stoichiometric amount of OsO_2 (Alfa Aesar, 99.99%) and Rb_2O (Aldrich, 99%) was thoroughly mixed in an argon filled dry box and pressed into pellets. The pellets were put to a quartz tube which was evacuated and sealed. The tube was heated up to 600°C and kept at this temperature for 24 h. According to the X-ray analysis, the resulting sample contained two phases, namely, pyrochlore RbOs_2O_6 and RbOsO_4 . RbOsO_4 was removed after 2 h etching in a 10% solution of HCl and sub-

sequent washing with water and drying at 100°C. The X-ray diffraction pattern of the post treated sample is shown in Fig. 1 where all reflections can be indexed on the basis of the pyrochlore cell with a lattice parameter $a=10.1137(1)$ Å.

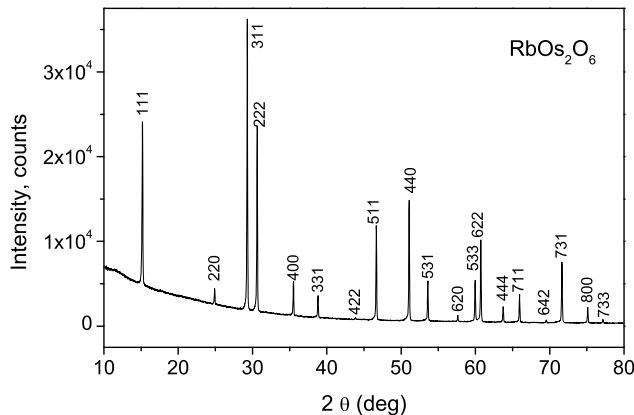


FIG. 1: X-ray diffraction pattern of the RbOs_2O_6 sample synthesized in a quartz tube. All reflections are indexed on the basis of the pyrochlore cell with a lattice parameter $a=10.1137(1)$ Å.

B. TF- μ SR

The μ SR experiments were performed at the π M3 beam line at the Paul Scherrer Institute (Villigen, Switzerland). The sample was field cooled from above T_c to 30 mK in fields of 2.5 T and 1 T, and to $\simeq 1.6$ K in a series of fields ranging from 5 mT to 0.6 T. We used the transverse field μ SR to probe the local magnetic field distribution $P(B)$ inside the superconducting sample in the mixed state. The second moment of $P(B)$ is connected directly with the magnetic field penetration depth λ .¹⁹

The μ SR signal was observed in the usual time-differential way by monitoring the positron rate from the μ^+ decay as a function of the elapsed μ^+ lifetime in the positron telescopes. The time dependence of the positron rate is given by the expression:²⁰

$$\frac{dN}{dt} = N_0 \frac{1}{\tau_\mu} e^{-t/\tau_\mu} [1 + aP(t)] + bg, \quad (1)$$

where N_0 is a normalization constant, bg is a time-independent background, $\tau_\mu = 2.19703(4) \times 10^{-6}$ s is the μ^+ lifetime, a is the maximum decay asymmetry for the particular detector telescope ($a \sim 0.18$ in our case) and $P(t)$ is the spin polarization of the muon ensemble:

$$P(t) = \int P(B) \cos(\gamma_\mu Bt + \phi) dB. \quad (2)$$

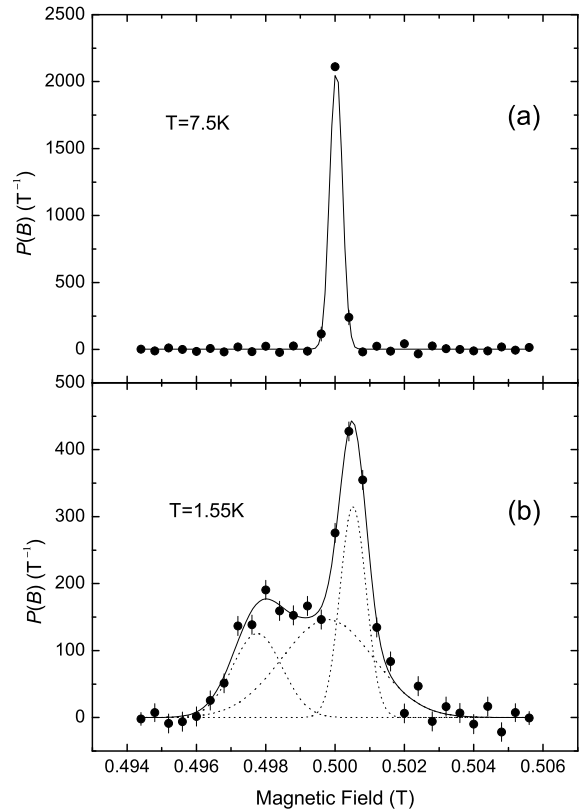


FIG. 2: Typical internal field distributions measured by the μ SR technique inside the RbOs_2O_6 sample above (a) and below (b) T_c after field cooling in a magnetic field of 0.5 T. Below T_c the field distribution is broadened and asymmetric. The lines represent the best fit with Gaussian line-shapes. See text for details.

Here $P(B)$ is the field distribution inside a sample, $\gamma_\mu = 2\pi \times 135.5342$ MHz/T is the muon gyromagnetic ratio and ϕ is the angle between the initial muon polarization and the effective symmetry axis of a positron detector. To link $P(t)$ and $P(B)$ one can use the algorithm of Fast Fourier Transform or the direct least square fit of $P(t)$ by the sum of precessions in discrete fields:²¹

$$P(t) = \sum_i A_i \cos(\gamma_\mu B_i t + \phi), \quad (3)$$

where A_i are varied and B_i are fixed with spacing $\Delta B \geq \pi/(\gamma_\mu t_{max})$, $t_{max} \sim 10^{-5}$ s is the time window of the μ SR technique.

Magnetic field distributions inside the RbOs_2O_6 sample in the normal (7.5 K) and the mixed (1.55 K) states after field cooling in a magnetic field of 0.5 T obtained by the procedure (3) are shown in Fig. 2. In the normal state, a single line at the position of the external magnetic field with broadening arising from the nuclear magnetic moments is seen. Below T_c the field distribu-

tion is broadened and asymmetric. For a better visualization, the fit of $P(B)$ by three Gaussian lines is represented by dotted lines in Fig. 2. Two wide lines with the mean frequencies below the external field are used to describe the asymmetric line shape in the superconducting part of the sample. The narrow line seen at a field a little bit above the external field suggests that part of the sample is in a normal state. The superconducting volume fraction is estimated to be $\simeq 70\%$ close to the specific heat measurements⁵ performed on a similarly synthesized sample where the superconducting fraction was estimated about 80%.

To obtain the second moment of the asymmetric field distribution in the superconducting state we used the procedure similar to Refs. [22,23]. All the μ SR spectra taken at $T < 0.85T_c$ where the three lines are resolved were analyzed by fitting a three component expression to the $P(t)$ data:

$$P(t) = A_b \exp(-\sigma_b^2 t^2 / 2) \cos(\gamma_\mu B_b t + \phi) + \sum_{i=1}^2 A_i \exp(-\sigma_i^2 t^2 / 2) \cos(\gamma_\mu B_i t + \phi), \quad (4)$$

The first term with small $\sigma_b < 0.3$ MHz and B_b close to the applied field corresponds to the background muons stopping in parts of the cryostat and in the nonsuperconducting parts of the sample. The sum corresponds to the asymmetric field distribution inside the superconductor. At $0.85T_c < T < T_c$ the two broad lines [see e.g Fig. (2)] responsible for superconducting state merge each other and the analysis is statistically correct for one superconducting signal. At $T > T_c$ the analysis is simplified to the background term only with $\sigma_b = \sigma_{nm} \sim 0.1$ MHz resulting from the nuclear moments of the sample.

The superconducting term in Eq. (4) is equivalent to the field distribution:

$$P(B) = \gamma_\mu \sum_{i=1}^2 \frac{A_i}{\sigma_i} \exp\left(-\frac{\gamma_\mu^2 (B - B_i)^2}{2\sigma_i^2}\right). \quad (5)$$

For this distribution the mean field and the second moment are^{22,23}

$$\langle B \rangle = \sum_{i=1}^2 \frac{A_i B_i}{A_1 + A_2} \quad (6)$$

and

$$\langle \Delta B^2 \rangle = \sum_{i=1}^2 \frac{A_i}{A_1 + A_2} [(\sigma_i / \gamma_\mu)^2 - [B_i - \langle B \rangle]^2]. \quad (7)$$

The extracted second moment of the magnetic field distribution of the vortex lattice can be expressed in frequency units

$$\sigma_{sc} = [\gamma_\mu^2 \langle \Delta B^2 \rangle - \sigma_{nm}^2]^{1/2}, \quad (8)$$

where σ_{nm} is the additional broadening due to the nuclear moments measured at $T > T_c$. The absolute value of λ is obtained from the relation

$$\sigma_{sc} [\mu\text{s}^{-1}] = 4.83 \times 10^4 (1-h) [1 + 3.9(1-h)^2]^{1/2} \lambda^{-2} [\text{nm}], \quad (9)$$

($h = H/H_{c2}$, and H_{c2} is the second critical field), which describes the field variation in an ideal triangular vortex lattice.¹⁹

In separating $P(B)$ in the signal from the superconductor and from the background by means of Gaussian functions by Eq. (4) a systematic error can occur. Part of the background signal may in fact be associated with the superconductor.²² We can estimate this error on the assumption that the entire signal described by Eq. (3) or Eq. (4) refers to the superconductor. In this case, the second moment of the whole $P(B)$ spectrum is systematically lower by 6.4% at $B = 0.1$ T, 5.4% at $B = 0.5$ T, 5.5% at $B = 1$ T, and 10.1% at $B = 2.5$ T. This may result to the systematic increase of λ by 3.2–5% respectively.

III. EXPERIMENTAL RESULTS AND DISCUSSION

A. Temperature dependence of λ

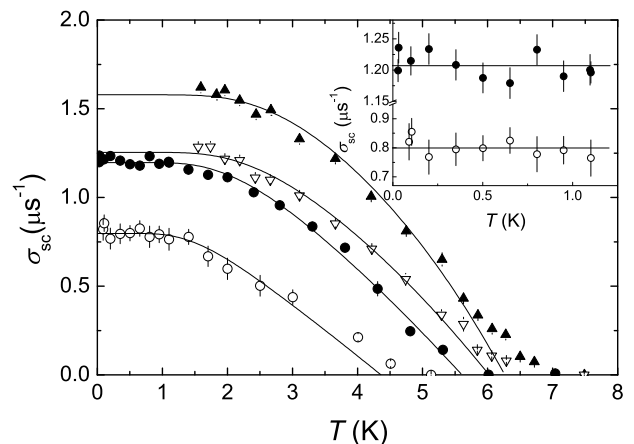


FIG. 3: Temperature dependence of $\sigma_{sc} \propto \lambda^{-2}$ of RbOs_2O_6 , measured in (from the top to the bottom) 0.1 T, 0.5 T, 1 T, and 2.5 T fields (field-cooled). The inset shows the low-temperature region between 0 K and 1.25 K. The constant (within the error bars) $\sigma_{sc}(T) \propto \lambda^{-2}$ suggests that RbOs_2O_6 is a weak-coupled BCS superconductor. Lines represent fit with the expression for the weak-coupling BCS model given in Eq. (10).

In Fig. 3 the temperature dependences of $\sigma_{sc} \propto \lambda^{-2}$ for $\mu_0 H = 0.1$ T, 0.5 T, 1 T, and 2.5 T are shown. For

$\mu_0 H = 1$ T and 2.5 T, $\sigma_{sc}(T)$ was measured down to 30 mK. It is seen that below 1.3 K (see inset in Fig. 3) λ^{-2} (σ_{sc}) is *temperature independent*. The experimental points are well fitted with $\sigma_{sc}(T) = \text{const}$. Note that the constant value of λ at low temperatures is predicted by the BCS model for weak-coupled superconductors.²⁴ The solid lines in Fig. 3 represent fit with the weak-coupling BCS model:²⁴

$$\frac{\lambda^{-2}(T, \Delta_0)}{\lambda^{-2}(0)} = 1 + 2 \int_{\Delta(T)}^{\infty} \left(\frac{\partial f}{\partial E} \right) \frac{E}{\sqrt{E^2 - \Delta(T)^2}} dE \quad (10)$$

Here, $f = [1 + \exp(E/k_B T)]^{-1}$ is the Fermi function, $\Delta(T) = \Delta_0 \hat{\Delta}(T/T_c)$ represents the temperature dependence of the energy gap, k_B is the Boltzman constant, and Δ_0 is the zero temperature value of the superconducting gap. For the normalized gap $\hat{\Delta}(T/T_c)$ values tabulated in Ref. [25] were used. The data in the Fig. 3 were fitted with $\sigma_{sc}(0)$ and Δ_0 as free parameters, and T_c fixed from the corresponding field-cooled magnetization (M_{FC}) measurements. T_c was obtained from the intersection of the linearly extrapolated $M_{FC}(T)$ curve in the vicinity of T_c with the $M = 0$ line (see inset in Fig. 5). All the present results of $\lambda(T)$ for RbOs_2O_6 are summarized in Table I.

TABLE I: Summary of the $\lambda(T)$ results (see text for details).

| $\mu_0 H$ (T) | T_c (K) | Δ_0 (meV) | $2\Delta_0/k_B T_c$ | $\sigma_{sc}(0)$ (μS^{-1}) | $\lambda(0)$ (nm) |
|------------------|--------------|---------------------|---------------------|--------------------------------------------|-----------------------------------------|
| 0.1 | 6.24(3) | 1.07(4) | 3.98(16) | 1.579(11) | 254(1) ^a 258(1) ^b |
| 0.5 | 6.00(4) | 0.93(3) | 3.60(12) | 1.254(10) | 270(2) ^a 290(1) ^b |
| 1 | 5.59(2) | 0.80(3) | 3.32(12) | 1.197(8) | 254(2) ^a 295(2) ^b |
| 2.5 | 4.36(2) | 0.58(5) | 3.09(27) | 0.797(8) | 232(7) ^a 355(4) ^b |

^a $H_{c2}(0)$ taken from the WHH model

^b $H_{c2}(0)$ taken from the fit of $H_{c2}(T)$ by means of the power law

In order to compare $\lambda(T)$ obtained in different fields (0.1 T, 0.5 T, 1 T, and 2.5 T) the normalized superfluid densities $\lambda^{-2}(T)/\lambda^{-2}(0) = \sigma(T)_{sc}/\sigma(0)_{sc}$ versus the reduced temperature T/T_c are plotted in Fig. 4. All $\lambda(T)$ collapse almost on one curve, indicating that the temperature dependences of λ^{-2} measured at different fields are nearly the same. This is in contrast to unconventional superconductors, as e.g. cuprate high-temperature superconductors,^{17,18,26,27} or the two-gap BCS-type MgB_2 superconductor,²⁸ where the shape of the temperature dependence of λ^{-2} varies with magnetic field. In cuprates, for example, this behavior can be explained by the different type of symmetry of the wave function at the surface and in the bulk (see e.g. [29]). In MgB_2 the field dependence of λ is explained by the fast suppression of the π band by the magnetic field (see

e.g. [30]). Thus, the observation of nearly the same temperature dependences of λ measured in different fields is an additional argument pointing to the conventional character of superconductivity in RbOs_2O_6 .

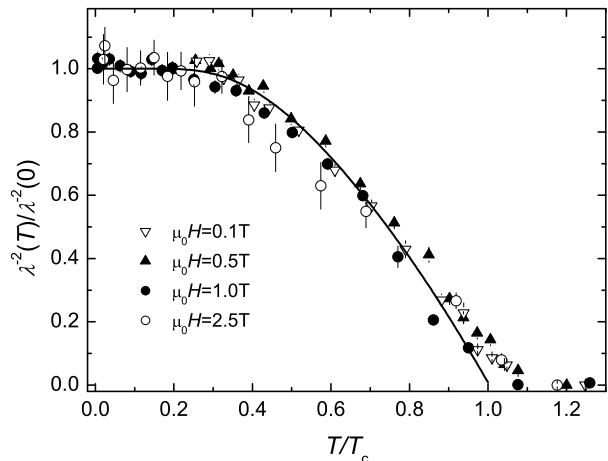


FIG. 4: Normalized superfluid density $\lambda^{-2}(T)/\lambda^{-2}(0) = \sigma_{sc}(T)/\sigma_{sc}(0)$ versus the reduced temperature T/T_c for 0.1 T, 0.5 T, 1 T, and 2.5 T. The solid line represents the fit of the 1 T μSR data with Eq. (10).

To summarize, in the whole temperature range (down to 30 mK) the temperature dependence of λ is consistent with what is expected for a weak-coupled s-wave BCS superconductor. The shape of $\lambda(T)$ is almost independent on the magnetic field.

B. The Zero Temperature Value of λ

To calculate the absolute value of $\lambda(0)$ from $\sigma_{sc}(0)$ one needs to know the zero temperature value of the second critical field $H_{c2}(0)$ [see Eq. (9)]. For this reason $H_{c2}(T)$ was extracted from the $M_{FC}(T)$ curves measured in constant magnetic fields ranging from 0.5 mT to 6 T (see Fig. 5). For each particular field H the corresponding $T_c(H)$ was taken as the temperature where $H = H_{c2}(T = T_c)$ (see inset in Fig. 5). H_{c2} depends almost linearly on T with some sign of saturation below 2.5 K. Note that a linear $H_{c2}(T)$ behavior was also observed in $\text{Cd}_2\text{Re}_2\text{O}_7$ ^{2,31} and recently in RbOs_2O_6 ,^{5,7} and in KOs_2O_6 ⁴ pyrochlore superconductors. In the conventional BCS picture, H_{c2} is linear in T near T_{c0} [$T_{c0} = T_c(H = 0)$] and saturates by approaching 0 K. The absolute value of $H_{c2}(0)$ can be obtained by using the Werthamer-Helfand-Hohenberg (WHH) formula³² proposed for a weak-coupling superconductor: $H_{c2}(0) = 0.693(-dH_{c2}/dT)|_{T=T_{c0}}$. The linear fit in the vicinity of T_{c0} yields $d\mu_0 H_{c2}/dT =$

$-1.37(4)$ T/K and $T_{c0} = 6.32(19)$ K. The corresponding value of $\mu_0 H_{c2}^{\text{WHH}}(0)$ was found to be $6.00(25)$ T. The dashed line in Fig. 5 is the theoretical $H_{c2}(T)$ curve obtained from the WHH model in the orbital limit.⁵ At high temperatures (above $\simeq 3.5$ K) the WHH line agrees rather well with the experimental data. However, at lower temperatures the experimental points no longer follow the WHH curve, suggesting that the actual value of $H_{c2}(0)$ is slightly larger than $H_{c2}^{\text{WHH}}(0)$. A

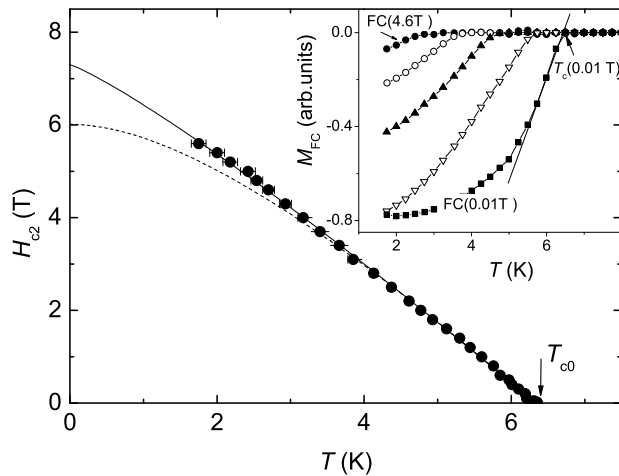


FIG. 5: H_{c2} vs T obtained from $M_{FC}(T)$ measurements (see text for details). The dotted line is $H_{c2}(T)$ obtained from the WHH model. The solid line is the fit with the power law $H_{c2}(T)/H_{c2}(0) = 1 - (T/T_{c0})^n$ with the parameters listed in the text. The inset shows M_{FC} vs T dependences after subtraction of the small paramagnetic background: from the left to the right $\mu_0 H = 4.6$ T, 3.4 T, 2.2 T, 1 T, and 0.01 T.

power law fit $H_{c2}(T)/H_{c2}(0) = 1 - (T/T_{c0})^n$ (solid line) gives an exponent $n = 1.17(5)$, $T_{c0} = 6.33(1)$ K, and $\mu_0 H_{c2}^{\text{PL}}(0) = 7.25(19)$ T. The values of $\lambda(0)$ calculated with $H_{c2}(0)$ obtained from the WHH model and from the fit with the power law are summarized in Table I. Finally, the representative range for $\lambda(0)$ in RbOs₂O₆ obtained from the μ SR experiments is 250-300 nm in agreement with the low-field magnetization measurements.¹³

C. The field dependence of λ

It is now well established that not only the temperature behavior, but also the field dependence of λ is completely different for conventional BCS-type and unconventional superconductors.^{11,17} By analyzing $\lambda(H)$ in different superconducting materials, it was concluded that in superconductors associated with an anisotropic energy gap λ increases almost linearly with the field.¹¹ This effect was

explained by the Doppler shift of the quasiparticles momentum in the gap nodes.^{11,17} It was also shown that in unconventional superconductors the slope

$$\eta = \frac{d[\lambda(h)/\lambda(0)]}{dh}, \quad (11)$$

($h = H/H_{c2}$) lies in a range of 1 to 6, while it is close to zero for superconductors with the isotropic energy gap.¹¹

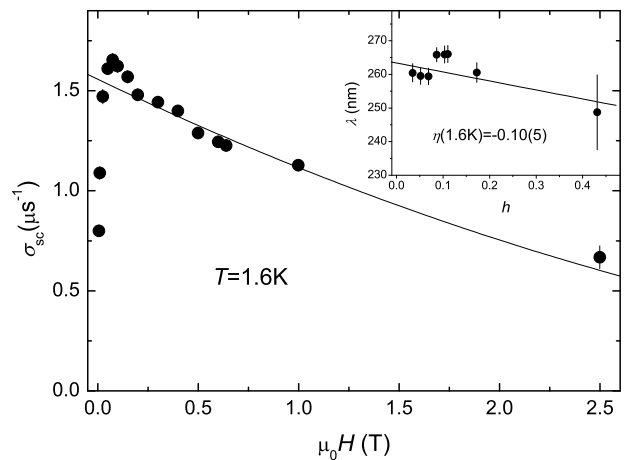


FIG. 6: Magnetic field dependence of σ_{sc} for RbOs₂O₆ measured at $T = 1.6$ K. Each point was obtained after field-cooling the sample from a temperature above T_c . The solid line is obtained from Eq. (9) with the parameters written in the text. The inset shows $\lambda(1.6$ K) as a function of $h = H/H_{c2}$.

In order to obtain the field dependence of λ , σ_{sc} was measured as a function of the magnetic field (see Fig. 6). Each point was obtained by field-cooling the sample from a temperature well above T_c to 1.6 K. The value of $\sigma_{sc}(H, 1.6$ K) increases almost linearly up to 75 mT; goes through a pronounced maximum around 0.1 T and then starts to decrease from $1.65 \mu\text{s}^{-1}$ at the peak position to $0.67 \mu\text{s}^{-1}$ at 2.5 T. The solid line is the theoretical $\sigma_{sc}(H)$ dependence obtained by means of Eq. (9) with $\mu_0 H_{c2}(1.6$ K) = $5.80(2)$ T [taken from the $H_{c2}(T)$ curve given in Fig. 5], and the field independent $\lambda(1.6$ K) = 262 nm. Above $\simeq 0.2$ T there is quite a good agreement between theory and experimental data. The deviations at lower fields are most probably determined by the distortion of the vortex lattice induced by pinning. A similar peak (followed by a plateau at high fields) is usually observed in high-temperature superconductors.^{33,34}

The inset in Fig. 6 shows the λ vs. h for $\mu_0 H > 0.2$ T at $T = 1.6$ K. A linear fit yields $\eta(1.6$ K) = $-0.10(5)$. The observation of a small η suggests that RbOs₂O₆ is a superconductor with an isotropic energy gap (see e.g. [11]).

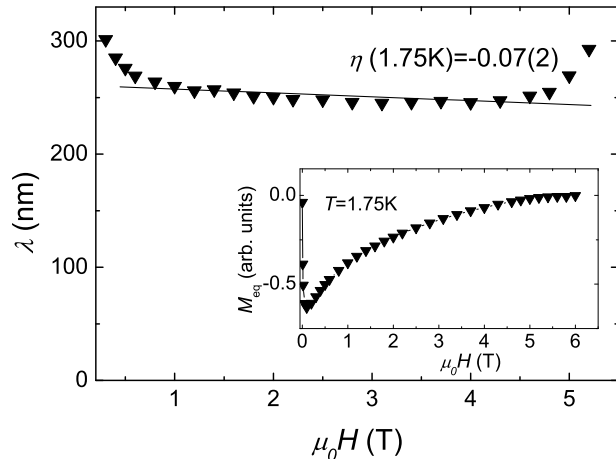


FIG. 7: The magnetic field dependence of the penetration depth λ of RbOs_2O_6 at $T = 1.75$ K, extracted from the measurements of the equilibrium magnetization (M_{eq}) shown in the inset. The solid line is the linear fit in the field region 0.6 T – 4.8 T.

We also performed additional λ vs. H experiments based on measurements of the equilibrium magnetization M_{eq} . Following Kogan *et al.* [35] one can write:

$$\lambda^{-2} \propto \frac{dM_{eq}}{d \ln H}. \quad (12)$$

This is the consequence of the London equation predicting that in type-II superconductor with zero pinning, the magnetization is proportional to $\lambda^{-2} \ln H$. Note that Eq. (12) is valid only in the intermediate field region $H_{c1} \ll H \ll H_{c2}$ (here H_{c1} is the first critical field).²⁴ To avoid the "pinning" problem, $M_{eq}(H)$ was taken from field-cooled measurements $M_{eq}(T, H) = M_{FC}(T, H)$ (see inset in Fig. 7). As shown above in our sample pinning (maximum in Fig. 6) is suppressed at fields above $\simeq 0.2$ T. The λ vs. H dependence, reconstructed by means of Eq. (12) and using the values of $M_{eq}(H)$ at $T = 1.75$ K is shown in Fig. 7. Because it is not possible to calculate the absolute value of λ from Eq. (12), data in Fig. 7 are scaled to the μSR value of $\lambda(1.75 \text{ K})$ at $\mu_0 H = 1$ T. It is seen that between 0.6 T and 4.8 T the λ vs H dependence is almost flat. A linear fit of the data in this field range yields a slope $\eta = -0.07(2)$, in agreement with the η value obtained from the μSR experiment.

To summarize, the magnetic penetration depth λ measured at low temperatures was found to be almost (within the accuracy of 10%) *field independent*. This suggests that the superconducting energy gap in RbOs_2O_6 is *isotropic*.

D. Dependence of the zero-temperature superconducting gap Δ_0 on the critical temperature and the magnetic field

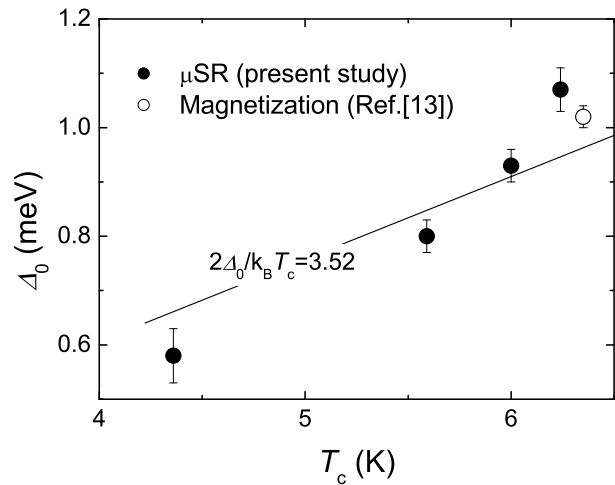


FIG. 8: Δ_0 vs. T_c in RbOs_2O_6 . The solid line represents the universal BCS line with $2\Delta_0/k_B T_c = 3.52$.

Bearing in mind that the critical temperature T_c is a function of the applied magnetic field, in Fig. 8 the zero-temperature superconducting gap Δ_0 (obtained from fits of the $\lambda^{-2}(T)$ data shown in Fig. 3) are plotted as a function of T_c . In addition we also include in this graph the value $\Delta_0(0.5 \text{ mT}) = 1.02(2)$ meV obtained from the magnetization measurements.¹³ The solid line represents the universal BCS line with $2\Delta_0/k_B T_c = 3.52$. It is seen that the experimental points are located close to the BCS line. However, at high and at low temperatures the data systematically deviate from the simple BCS line, suggesting that the ratio $2\Delta_0/k_B T_c$ is field dependent as demonstrated in Fig. 9. It is worth noting that for conventional bulk superconductors the ratio $2\Delta_0/k_B T_c$ is field independent, while in thin films and in granular materials the dependence is quite strong.²⁴ For the thin films of Sn, Pb and In^{37,38} it was experimentally observed that at the low temperatures the magnetic field dependence of the BCS ratio follows the empirical relation:

$$\frac{2\Delta_0(H)}{k_B T_c(H)} = \frac{2\Delta_0(0)}{k_B T_c(0)} \left[1 - (H/H_{c2})^2 \right], \quad (13)$$

where $2\Delta_0(0)/k_B T_c(0)$ is the BCS ratio at zero field. The shadowed region in Fig. 9 represents the results of calculations by means of Eq. 13 with $2\Delta_0(0)/k_B T_c(0) = 3.72$ and assuming that $H_{c2}(0)$ lies between the values obtained from the WHH model and from the fit with the power law (see Sec. III B). The field dependence of the

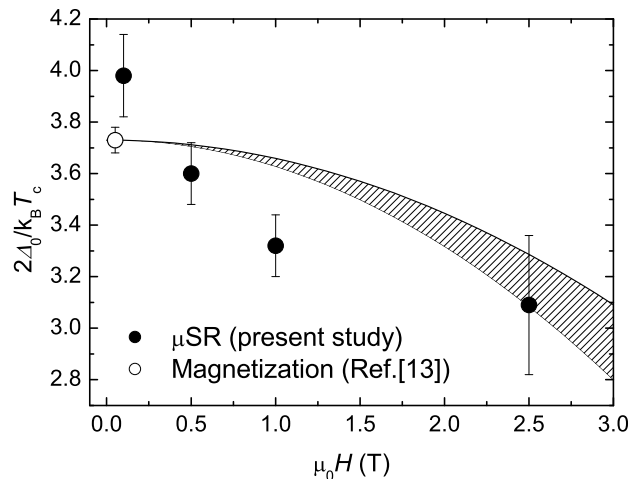


FIG. 9: Field dependence of the BCS ratio $2\Delta_0/k_B T_c$. The shadowed region represents the $2\Delta_0(H)/k_B T_c(H)$ obtained from Eq. (13) with $H_{c2}^{\text{WHH}}(0) \leq H_{c2}(0) \leq H_{c2}^{\text{PL}}(0)$.

energy gap may be explained if one assumes that the electrons moving close to the surface contribute less to the pairing energy.³⁶ This may result to the decrease of the energy gap with increasing the magnetic field.

To summarize, the ratio $2\Delta_0/k_B T_c$ is found in the range of 3.09–3.98 close to the weak-coupling BCS value 3.52. The field dependence of this ratio can be explained by the finite size of the individual grains of the sample.

IV. CONCLUSIONS

Muon-spin rotation and magnetization studies were performed on the pyrochlore superconductor RbOs_2O_6 .

The main conclusions are: (i) The absolute value of λ at zero temperature obtained from μSR experiments is in the range from 250 nm to 300 nm. (ii) In the temperature region down to 30 mK the temperature dependence of λ is consistent with what is expected for a weak-coupled s-wave BCS superconductor. (iii) The shape of $\lambda(T)$ is almost independent of the magnetic field. (iv) The value of the zero-temperature superconducting gap decreases with increasing magnetic field (decreasing of T_c). The ratio $2\Delta_0/k_B T_c$ was found to be in the range of 3.09–3.98 close to the weak-coupling BCS value 3.52. (v) The μSR and the equilibrium magnetization measurements both show that at low temperatures the magnetic penetration depth λ is almost (within the accuracy of 10%) field independent, in agreement with what is expected for a superconductor with an isotropic energy gap. To conclude, all the above mentioned features suggest that RbOs_2O_6 is a weak-coupled BCS superconductor with an isotropic energy gap.

V. ACKNOWLEDGMENTS

This work was partly performed at the Swiss Muon Source ($S\mu\text{S}$), Paul Scherrer Institute (PSI, Switzerland). The authors are grateful to A. Amato and D. Herlach for providing beam-time within the PSI short-term proposal system. This work was supported by the Swiss National Science Foundation and by the NCCR program *Materials with Novel Electronic Properties* (MaNEP) sponsored by the Swiss National Science Foundation.

¹ M. Hanawa, Y. Muraoka, T. Tayama, T. Sakakibara, J. Yamamura, and Z. Hiroi, Phys. Rev. Lett. **87**, 187001 (2001).
² H. Sakai, K. Yoshimura, H. Ohno, H. Kato, S. Kambe, R.E. Walstedt, T.D. Matsuda, Y. Haga, and Y. Onuki, J. Phys.: Cond. Mat. **13**, L785 (2001).
³ S. Yonezawa, Y. Muraoka, Y. Matsushita, and Z. Hiroi, J. Phys.: Cond. Mat. **16**, L9 (2004).
⁴ Z. Hiroi, S. Yonezawa, and Y. Muraoka, J. Phys. Soc. Jpn **73**, 1651 (2004).
⁵ M. Brühwiler, S.M. Kazakov, N.D. Zhigadlo, J. Karpinski, and B. Batlogg, Phys. Rev. B **70**, 020503(R) (2004).
⁶ S.M. Kazakov, N.D. Zhigadlo, M. Brühwiler, B. Batlogg, and J. Karpinski, Supercond. Sci. Technol. **17**, 1169 (2004).
⁷ S. Yonezawa, Y. Muraoka, Y. Matsushita, and Z. Hiroi,

J. Phys. Soc. Jpn **73**, 819 (2004).
⁸ S. Yonezawa, Y. Muraoka, and Z. Hiroi, J. Phys. Soc. Jpn **73**, 1655 (2004).
⁹ Z. Hiroi and M. Hanawa, J. Phys. Chem. Solids **63**, 1021 (2002).
¹⁰ O. Vyaselev, K. Kobayashi, K. Arai, J. Yamazaki, K. Kodama, M. Takigawa, M. Hanawa, and Z. Hiroi, J. Phys. Chem. Solids **63**, 1031 (2002).
¹¹ R. Kadono, J.Phys.: Cond.Mat. **16**, S4421 (2004).
¹² M.D. Lumsden, S.R. Dunsiger, J.E. Sonier, R.I. Miller, R.F. Kiefl, R. Jin, J. He, D. Mandrus, S.T. Bramwell, and J.S. Gardner, Phys. Rev. Lett. **89**, 147002 (2001).
¹³ R. Khasanov, D.G. Eshchenko, J. Karpinski, S.M. Kazakov, N.D. Zhigadlo, R. Brühwiler, D. Gavillet, D. Di Castro, A. Shengelaya, F. La Mattina, A. Maisuradze, C. Baines,

- and H. Keller, Phys. Rev. Lett. **93**, 157004 (2004).
- ¹⁴ K. Magishi, J.L. Gavilano, B. Pedrini, J. Hinderer, M. Weller, H.R. Ott, S.M. Kazakov, J. Karpinski, cond-mat/0409169.
- ¹⁵ R. Saniz, J.E. Medvedeva, Lin-Hui Ye, T. Shishidou, and A.J. Freeman, Phys. Rev. B **70**, 100505(R) (2004).
- ¹⁶ A. Koda, W. Higemoto, K. Ohishi, S.R. Saha, R. Kadono, S. Yonezawa, Y. Muraoka, and Z. Hiroi, cond-mat/0402400.
- ¹⁷ J. Sonier, J. Brewer, and R. Kiefl, Rev. Mod. Phys. **72**, 769 (2000).
- ¹⁸ P. Zimmermann, H. Keller, S. L. Lee, I. M. Savic, M. Warden, D. Zech, R. Cubitt, E. M. Forgan, E. Kaldis, J. Karpinski, and C. Krüger, Phys. Rev. B **52**, 541 (1995).
- ¹⁹ E.H. Brandt, Phys. Rev. B **37**, R2349 (1988).
- ²⁰ A. Schenck, *Muon Spin Rotation: Principles and Applications in Solid State Physics*, (Adam Hilger, Bristol, 1986); S.F.J. Cox, *J. Phys.* **C20**, 3187 (1987); J.H. Brewer, "Muon Spin Rotation/Relaxation/Resonance" in *Encyclopedia of Applied Physics* Vol. 11, p. 23 (VCH, New York, 1995).
- ²¹ V. Pomjakushin, Private communications.
- ²² V.G. Grebinnik, V.N. Duginov, V.A. Zhukov, B.F. Kirilov, N.M. Kotov, V.I. Kudinov, T.N. Mamedov, B.A. Nikol'skiĭ, Yu.V. Obukhov, V.G. Ol'shevskii, A.V. Pirogov, V.Yu. Pomyakushin, A.N. Ponomarev, G.I. Savel'ev, V.A. Suetin, and V.G. Firsov, Phys. At. Nucl. **56**, 443 (1993).
- ²³ M. Weber, A. Amato, F.N. Gigax, A. Schenck, M. Maletta, V.N. Duginov, V.G. Grebinnik, A.B. Lazarev, V.G. Olshvsky, V.Yu. Pomjakushin, S.N. Shilov, V.A. Zhukov, B.F. Kirilov, A.V. Pirogov, A.N. Ponomarev, V.G. Storchak, S. Kapusta, and J. Bock, Phys. Rev. B **48**, 13022 (1993).
- ²⁴ M. Tinkham, "Introduction to Superconductivity", *Krieger Publishing company, Malabar, Florida, 1975*.
- ²⁵ B. Mühlischlegel, Z. Phys. **155**, 313 (1959).
- ²⁶ W.N. Hardy, D.A. Bonn, D.C. Morgan, R. Liang, and K. Zhang, Phys. Rev. Lett. **70**, 3999 (1993).
- ²⁷ R. Khasanov *et al.* unpublished.
- ²⁸ Ch. Niedermayer, C. Bernhard, T. Holden, R.K. Kremer, and K. Ahn, Phys. Rev. B **65**, 094512 (2002).
- ²⁹ K.A. Müller, Phil. Mag. Lett. **82**, 279 (2002).
- ³⁰ M. Angst, D.Di Castro, D.G. Eshchenko, R. Khasanov, S. Kohout, I.M. Savic, A. Shengelaya, S.L. Bud'ko, P.C. Canfield, J. Jun, J. Karpinski, S.M. Kazakov, R.A. Ribeiro, and H. Keller, cond-mat/0405495.
- ³¹ R. Jin, J. He, S. McCall, C.S. Alexander, F. Drymiotis, and D. Mandrus, Phys. Rev. B **64**, 180503(R) (2001).
- ³² N.R. Werthamer, E. Helfand, and P.C. Hohenberg, Phys. Rev. **147**, 295 (1966).
- ³³ B. Pümpin, H. Keller, W. Kündig, W. Odermatt, I.M. Savic, J.W. Schneider, H. Simmler, P. Zimmermann, E. Kaldis, S. Rusiecki, Y. Maeno, and C. Rossel, Phys. Rev. B **42**, 8019 (1990).
- ³⁴ Ch. Niedermayer, C. Bernhard, U. Binniger, H. Glückler, J.L. Tallon, E.J. Ansaldo, and J.I. Budnick, J. Supercond. **7**, 165 (1994).
- ³⁵ V.G. Kogan, M.M. Fang, and S. Mitra, Phys. rev. B. **38**, R11958 (1988).
- ³⁶ Y. Nambu and S.F. Tuan, Phys. Rev. Lett. **11**, 119 (1963); Phys. Rev. **133**, A1 (1964).
- ³⁷ D.E. Morris and M. Tinkham, Phys. Rev. **134**, A1154 (1964).
- ³⁸ R. Meservey and D.H. Douglass, Jr., Phys. Rev. **135**, A24 (1964).